ACS SENSORS

Article

Cite This: ACS Sens. 2017, 2, 1602-1611

pubs.acs.org/acssensors

Structural Disruption of an Adenosine-Binding DNA Aptamer on Graphene: Implications for Aptasensor Design

Zak E. Hughes and Tiffany R. Walsh*

Institute for Frontier Materials, Deakin University, Geelong, Victoria 3216, Australia

Supporting Information

ABSTRACT: We report on the predicted structural disruption of an adenosine-binding DNA aptamer adsorbed via noncovalent interactions on aqueous graphene. The use of surface-adsorbed biorecognition elements on device substrates is needed for integration in nanofluidic sensing platforms. Upon analyte binding, the conformational change in the adsorbed aptamer may perturb the surface properties, which is essential for the signal generation mechanism in the sensor. However, at present, these graphene-adsorbed aptamer structure(s) are unknown, and are challenging to experimentally elucidate. Here we use molecular dynamics simulations to investigate the structure and analyte-binding properties of this aptamer, in the presence and absence of adenosine, both free in solution and adsorbed at the aqueous graphene interface. We predict this aptamer to support a variety of stable binding modes, with direct base−graphene contact arising from regions located in the terminal bases, the centrally located binding pockets, and the distal loop region. Considerable retention of the in-solution aptamer structure in the adsorbed state indicates that strong intra-aptamer interactions compete with the graphene−aptamer interactions. However, in some adsorbed configurations the analyte adenosines detach from the binding pockets, facilitated by strong adenosine−graphene interactions.

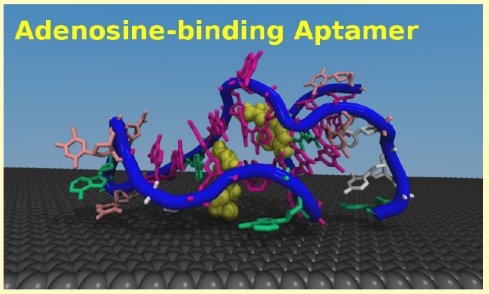

KEYWORDS: *DNA, aptamer, graphene, adenosine, molecular simulation, aptasensor*

The identification of aptamers, oligonucleotide sequences that are able to bind to particular small-molecule ligands with a high affinity and specificity,[1−4] offers promising routes for the development of new biosensors and clinical applications.[5,6] In many of these applications, integration of the aptamer with a surface/substrate is a necessary requirement.[7−10] One substrate that is particularly promising is graphene, with its many desirable properties such as conductivity, flexibility, and transparency.[8,10,11] However, to advance the development of aptamer/graphene-based sensing platforms, a well-developed understanding of how the molecular structure of the aptamer may be affected by the presence of the substrate, in the presence and the absence of the target analyte, is needed. In particular, the question of whether the substrate might degrade the aptamer structure and possibly reduce the aptamer binding affinity and/or selectivity is critical. To elaborate, in many instances, aptamer-based biosensors rely on realizing a reliable conformational response of the aptamer upon binding of the target analyte. While this conformational response might be predictable when the aptamer is free in solution (i.e., in the absence of the sensor substrate), the presence of the substrate may give rise to complications. In particular, at present it is not uncommon for new aptamer-based sensor platform designs to suffer from inconsistent and/or unreliable behaviors, which are challenging to diagnose, and therefore resolve, without a deeper comprehension of the conformational response of the aptamer when localized near the substrate interface. Moreover, the incorporation of reporter molecules (such as fluorophores) into the aptamer structure may also further hinder the interpretation of aptasensor data, without clear guidance on how these modifications affect the conformational traits of the surface-adsorbed aptamer.

Considering the aromatic character of both the nucleobases and graphitic substrates, it is not surprising that previous studies indicate a strongly favorable interaction between the two.[11−22] However, despite the strong favorable interaction with graphene at the nucleobase level, the greater macromolecular structure of an oligonucleotide may play a pivotal role in governing how the aptamer interacts with the aqueous graphitic interface. This phenomenon may, for example, result in the different behavior reported for the interaction of ssDNA and dsDNA with solid surfaces. With a highly flexible backbone and lack of defined secondary structure, ssDNA is thought to bind strongly to graphene and carbon nanotube (CNT) substrates.[12,14,16,18−21,23,24] Accordingly, the consensus prediction from molecular dynamics (MD) simulations is that ssDNA adsorbs in a flat conformation with a majority of the nucleobases in direct contact with the substrate, although interbase interactions have been found to be important in some cases.[22−29] In contrast, dsDNA (and regions of ssDNA possessing well-defined secondary structure) tend to interact

Received: June 28, 2017
Accepted: October 24, 2017
Published: October 24, 2017

DOI: 10.1021/acssensors.7b00435
ACS Sens. 2017, 2, 1602−1611

more weakly with CNTs and graphene, with the interfacial molecular structure relatively less affected by the adsorption process.[11,18,20,27,29−32] Also, the molecular-level structure of the interaction of dsDNA/dsRNA with graphene interfaces appears less clear than in the case of ssDNA, with previously proposed surface-binding modes of dsDNA including an upright orientation via surface contact with the 3′ and 5′ terminal bases, or in a parallel orientation.[27,29,30,32,33] Overall, the interaction of oligonucleotides with graphitic substrates therefore depends on the balance between nucleotide base pairing, nucleotide $\pi-\pi$ interactions, backbone flexibility, and nucleotide−substrate $\pi-\pi$ interactions. In many instances, DNA aptamers may contain both regions of dsDNA and ssDNA, and therefore the molecular-scale details of the aptamer−graphene interaction may depend strongly on the nature of the aptamer.

The DNA aptamer ACCTGGGGGAGTATTGCGGAGGAAGGT has been shown to bind adenosine, adenosine triphosphate (ATP), and adenosine monophosphate (AMP) at micromolar concentrations.[34] The ability to detect small variations in AMP levels under physiological conditions is highly relevant to a range of health conditions, including diabetes and obesity. The three-dimensional solution structure of this aptamer when complexed with two adenosine molecules (herein referred to as the *holo* form) has been reported based on nuclear magnetic resonance (NMR) spectroscopy studies (PDB-ID: 1AW4), while free in solution (i.e., in the absence of a solid surface).[34,35] Four Watson−Crick (WC) base pairs are present in the duplexed stem of aptamer, followed by a guanine-rich region containing two nonequivalent ligand binding pockets, located at G9 and G22, and then finally two more base pairs (one WC, one mismatch) and a small trimeric loop (A13-T14-T15) at the distal end of the aptamer. While the structure of the *holo* form is well characterized, there are still some questions over the degree of conformational change in the absence of the analyte. Previous NMR studies suggested only minor conformational changes upon ligand binding,[35] a conclusion supported by quartz-crystal microbalance (QCM) experiments of biotinylated aptamers deposited on sensors.[9] However, this finding may not be consistent with single-pair Förster resonance energy transfer (spFRET) spectroscopy measurements that indicate the ligand-free form (herein referred to as the *apo* form) resembles that of the *holo* form under high salt concentrations, while suggesting that at low salt concentrations the *apo* aptamer is more dynamic, preferring an unfolded conformation.[36] Moreover, very recent studies indicate that the binding of the target into the two binding pockets is only weakly cooperative, with single-pocket variants of this aptamer binding with similarly high binding affinity and specificity.[37]

Recently, the use of this aptamer, via physical adsorption onto graphene substrates, has yielded a successful demonstration of a proof-of-concept field-effect-transistor (FET)-like electromechanical biosensor device for the detection of ultralow concentrations of AMP.[38] However, in this device the authors used a pyrene tag placed at the 5′ end, which may have influenced the adenosine-binding capabilities of the aptamer. Despite this encouraging progress, the systematic improvement of such devices hinges on our ability to monitor, elucidate, and manipulate the structure of such aptamers when adsorbed at the aqueous graphene interface. However, the task of clearly elucidating the molecular-level structure(s) of biomolecules adsorbed to solid surfaces under aqueous conditions remains challenging. Therefore, in comparison with the current uncertainty regarding the molecular-level of the structure of the *apo* form, it is likely that an even greater degree of uncertainty may hinder our ability to determine these surface-adsorbed aptamer structures.

Currently, experimental data regarding the graphene adsorption properties of this aptamer are scarce. Fluorescent measurements of this aptamer physisorbed to the aqueous graphene oxide interface indicated that this aptamer retained selective binding of ATP, but also suggested a degree of conformational change in the molecule.[10] However, we note here that these experiments were conducted for the graphene oxide substrate, which might yield very different outcomes than those generated for a graphene substrate. Furthermore, recent experimental efforts based on atomic force microscopy (AFM), namely, single molecule force spectroscopy (SMFS), investigated the interaction of this aptamer with the aqueous graphite interface.[21] These SMFS experiments showed that by pulling the surface-adsorbed aptamer from aqueous graphite interface[12,16,18,20] this produced a stable force plateau in the measured force−distance curves, which can be interpreted as representing the successive, base-by-base desorption of the strand from the surface. Moreover, previous SMFS measurements of dsDNA at aqueous graphite interfaces reported a relatively reduced level of force required to remove the molecule from the substrate.[18,20] It may be viewed as perhaps counterintuitive that the peeling force required to pull the aptamer from the aqueous graphite interface was measured to be ∼40% higher in the presence of adenosine compared with that measured in the absence of adenosine.[21] These data suggest that the *holo* form interacted more strongly with the substrate than the *apo* form.

Given the challenge of obtaining experimental structural data at the relevant length scale for these surface-adsorbed aptamers under aqueous conditions, MD simulations comprise an alternative that can provide complementary information. Relatively few simulation studies have been published to date regarding aptamer adsorption at aqueous/solid interfaces, but there is a significant body of work on the interaction of DNA/RNA oligomers in general at the aqueous/solid interfaces for substrates such as gold,[39−42] graphene and/or CNTs,[22−30,32,43−46] and others.[47−49] As mentioned earlier, MD simulations have suggested very different adsorption modes for ssDNA compared with dsDNA at graphene interfaces, with dsDNA thought to undergo far less conformational change upon adsorption.[27,29,30,32]

Here, we have used MD simulations to investigate the structure of a DNA aptamer, in both the *apo* and *holo* forms, both free in solution and when adsorbed at the aqueous graphene interface. We chose to model the graphene substrate, as opposed to the graphene oxide substrate, because the bulk of the available experimental evidence has been obtained for aqueous graphite and graphene interfaces.[21,38] In the absence of the surface, we found that both forms possessed a strong degree of secondary structure, and that the structure of the aptamer did not unravel completely in the *apo* form. When adsorbed at the graphene interface, a variety of different adsorbed configurations were predicted.

METHODS

Simulation Details. The DNA aptamer and adenosine molecules were described using the CHARMM27 force-field (FF),[50,51] with the modified TIP3P model used to represent water molecules.[52,53] The interactions of water and aptamers with the graphene interface was

DOI: 10.1021/acssensors.7b00435
ACS Sens. 2017, 2, 1602−1611

described using the polarizable GRAPPA FF.[54] The performance of this force-field combination, in terms of recovering the free energy of adsorption at the aqueous DNA/graphene interface, was recently checked against SMFS experimental data on the nucleobase, nucleoside, and nucleotide levels.[55]

The initial structure of the 1AW4 aptamer was taken from the protein database (PDB-ID: 1AW4).[35] The *apo* and *holo* forms of the aptamer were simulated in bulk solution and at the aqueous graphene interface. In all cases the aptamer was simulated in 0.05 mol kg^{-1} NaCl (the same salt concentration used for the SMFS measurements of the molecule[21]). The bulk solution simulations consisted of the aptamer, and in the *holo* form, two adenosine molecules, and ∼23 800 water molecules in a ∼ 89.4 × 89.4 × 89.4 $Å^3$ simulation cell. The surface-adsorbed simulations systems comprised the aptamer (and in the *holo* form, two adenosine molecules) and ∼23 800 water molecules in the presence of a graphene sheet ∼88.5 × 89.5 $Å^2$, with a 93.5 Å distance separating the sheet from its periodic image along the cell direction perpendicular to the graphene surface plane.

All simulations were performed using Gromacs 5.0.[56] The Lennard-Jones nonbonded interactions were smoothly tapered to zero between 10.0 and 11.0 Å, and the electrostatic interactions were evaluated using a particle-mesh Ewald summation,[57] with a real space cutoff of 11.0 Å. The bulk solution simulations were performed in the isothermal−isobaric (*NpT*) ensemble, and for the adsorbed systems in the Canonical (*NVT*) ensemble was used. The Nosé−Hoover thermostat[58,59] and Parrinello−Rahman barostat[60] (for the bulk solution simulations) were used to maintain the temperature and pressure at 300 K and 1 atm, respectively. For the bulk solution systems, isotopic pressure coupling was applied. An integration time step of 1 fs was used for all simulations.

Two independent 250 ns simulations were performed for each form (*apo* and *holo*) in bulk solution. For the surface-adsorbed systems, each form was simulated starting from two different initial orientations: **Up**, where the binding pockets were directed away from the graphene surface and exposed to the bulk solution, and **Down**, where the binding pockets (plus adenosine molecules in the *holo* form) were directed toward the graphene sheet, as shown in Figure 1. For each system (*apo* up, *apo* down, *holo* up, *holo* down) two independent 300 ns simulations were performed. Both the initial velocities and the initial coordinates were different for every simulation run.

We anticipate that the aptamer will feature a complex potential energy landscape, particularly in the surface-adsorbed state, which means that even 250/300 ns of standard MD simulation may not be sufficient to ensure that the system does not become trapped in high-energy (metastable) minima. As such, in addition to performing the above simulations at 300 K, a further set of simulations was also performed, where after 100 ns (50 ns for the solution systems) at 300 K, the system was subjected to a series of simulated annealing (SA) cycles. Each SA cycle consisted of heating the system from 300 to 400 K over 0.5 ns, 2 ns at 400 K, and a 2.5 ns period where the system was cooled from 400 back to 300 K. During the SA cycle the volume of the system was kept constant. Each surface-adsorbed and bulk solution simulation was subjected to 10 and 5 SA cycles, respectively. At the conclusion of these SA cycles, the adsorbed/solution systems were subjected to a further 150/175 ns of simulation at 300 K, respectively. A complete summary of the simulations reported in this work is provided in Table S1 of the Supporting Information.

Analysis. For each simulation run the root-mean square deviation (RMSD) of the positions of the atoms in the backbone, the number of DNA nucleobase-nucleobase hydrogen bonds, and the stacking number of the aptamer as a function of simulation time were calculated. For the simulations of the *holo* form, the center of mass distance between each of the adenosine molecules and the aptamer over the course of the simulation was also calculated. In the case of the graphene-adsorbed systems, the number of nucleobases directly adsorbed at the surface as a function of simulation time was also calculated. Each of these metrics was block averaged over 5 ns periods.

The stacking number of the aptamer was determined as outlined by Portella and Orozco.[61] A base was considered adsorbed if the center of mass of the ring (for the pyrimidines), or the midpoint of the bond between the two rings (for the purines), was located within 4.2 Å of the graphene surface. This distance was assigned based on distance distribution profiles as described in previous studies.[62]

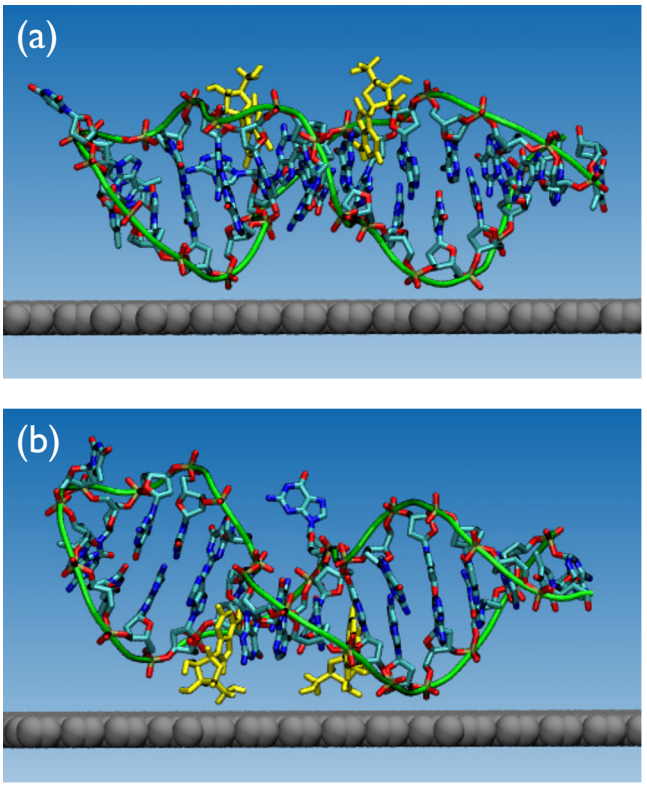

Figure 1. Snapshots showing the (a) **Up** and (b) **Down** orientations. Water molecules and hydrogen atoms are not shown for clarity. Color code: adenosine molecules in yellow, graphene surface in gray, aptamer backbone in green, while the carbon, nitrogen, and oxygen atoms of the aptamer are colored cyan, blue, and red, respectively.

RESULTS AND DISCUSSION

Simulations of the Aptamer in Solution. Figure 2 summarizes the MD simulation results for different bulk solution systems, averaged over the two runs, for each system. A breakdown of these results for each individual run is provided in Figures S1 and S2 of the Supporting Information. Even after 250 ns of MD simulation, the control runs of both the *holo* and the *apo* forms revealed only minor differences compared with the initial aptamer structure, as illustrated by the representative configurations provided in Figure S3 of the Supporting Information. The backbone RMSD of the *holo* form did not vary significantly over the course of the control runs, and that of the *apo* form showed only a minor increase in backbone RMSD. Similarly, the number of nucleobase−nucleobase hydrogen bonds and the stacking number were broadly unchanged. Application of the SA procedure to the DNA yielded more substantial changes to the base−base interactions of the aptamer, with a reduction in the number of stacked bases and the number of base−base hydrogen bonds, especially for the *apo* form. In turn, this disruption to the intramolecular interactions facilitated a greater degree of change to the aptamer backbone structure compared with the control runs. That said, the final structures of the aptamer still resembled those of the initial aptamer structure quite closely, as illustrated in Figure 3. A broader selection of representative snapshots of

DOI: 10.1021/acssensors.7b00435
ACS Sens. 2017, 2, 1602−1611

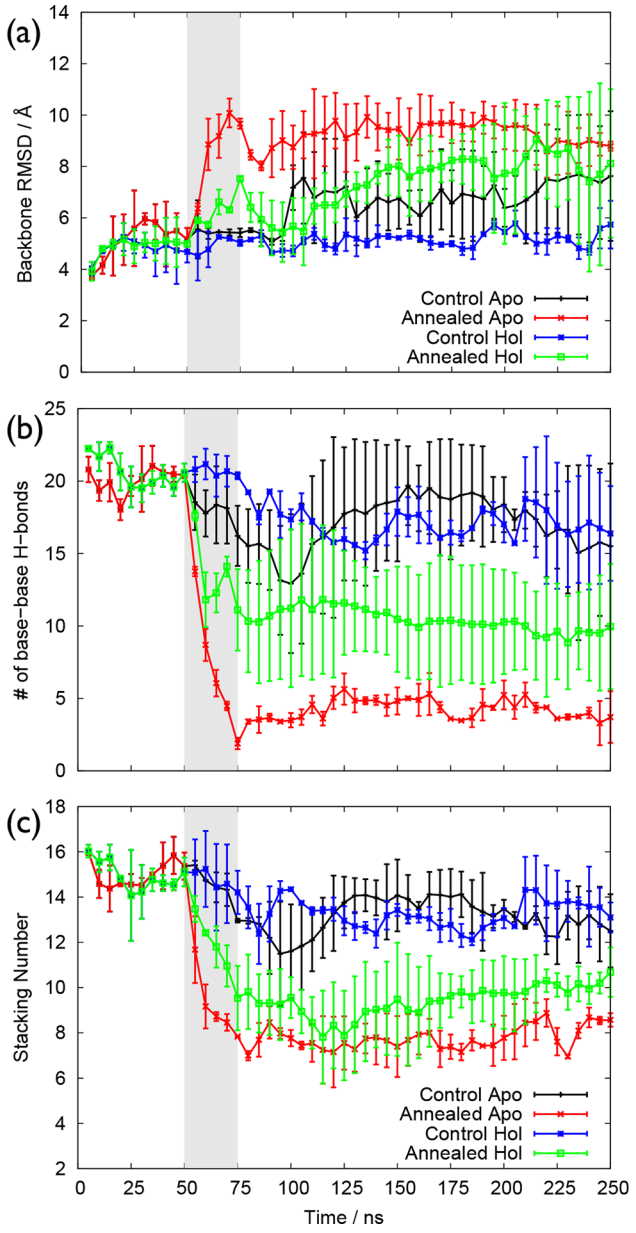

Figure 2. Data for DNA aptamer in solution, averaged over two runs for each system: (a) the RMSD of the aptamer backbone atoms, (b) the number of DNA nucleobase−nucleobase hydrogen bonds, and (c) the base stacking number as a function of simulation time. The shaded area indicates the period where the simulated annealing protocol was applied to the annealed runs.

the final configurations from the annealed runs is provided in Figure S4 of the Supporting Information.

For the control runs, all four of the adenosine molecules remained bound to the aptamer over the course of the simulations. For the SA runs, one adenosine molecule (out of the four) escaped the binding pocket of the aptamer. However, in this instance the adenosine still remained bound to the aptamer (on the exterior of the binding pocket), suggesting that the SA procedure did not disrupt the aptamer to such an extent so as to completely expel the bound ligands.

Overall, these data indicate that the structure of the aptamer in solution is highly stable, and even when exposed to the SA procedure maintained a strong structural integrity. These results are also consistent with the majority of experimental

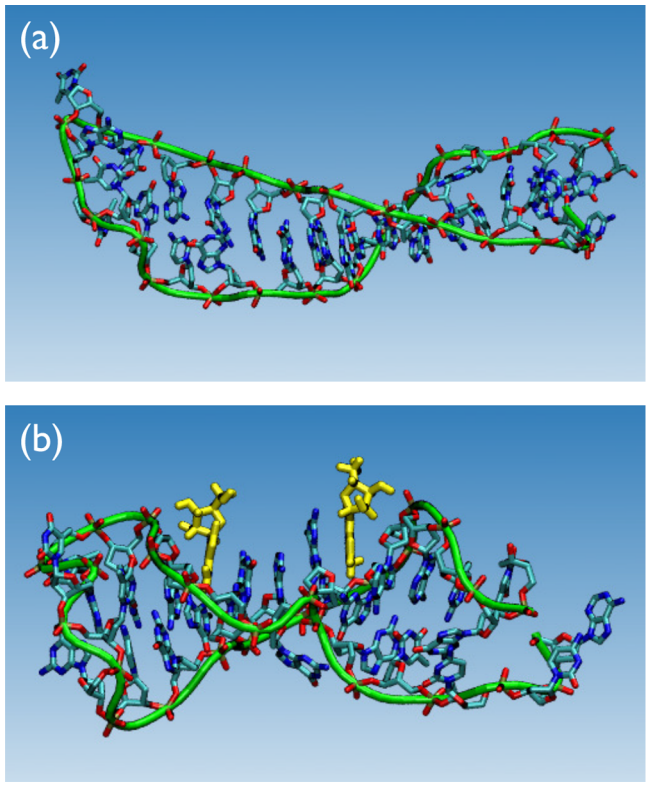

Figure 3. Snapshots of representative aptamer configurations in bulk solution for (a) the *apo* and (b) the *holo* form annealing runs. Water molecules and hydrogen atoms in the aptamer are not shown for clarity. Color code: adenosine in yellow, aptamer backbone in green, while the carbon, nitrogen, and oxygen atoms of the aptamer are colored cyan, blue, and red, respectively.

evidence, with the consensus view that the conformation of the *apo* form remained folded and resembled the *holo* form.

Aptamer Adsorption at the Aqueous Graphene Interface. Figure 4 shows the number of nucleobases adsorbed to the aqueous graphene interface as a function of simulation time for the control (i.e., unannealed) simulation runs. The nucleobases adsorbed in a stepwise fashion, as is characteristic of adsorption of nucleobases at graphitic surfaces, with very few nucleobase desorption events noted here. After 300 ns of control simulation, most systems featured only a relatively small proportion of adsorbed bases, between 7% and 5%. However, there was a substantial degree of variation in this metric, even between runs of the same system, making it challenging to conclusively determine any effect of initial orientation (up or down) or form (i.e., *apo* or *holo*), although there is some suggestion that a greater number of bases might be adsorbed for the *holo* form. Subjecting the aptamer to the SA process disrupted the internal structure of molecule and thus encouraged further adsorption of the nucleobases, as shown in Figure 5. While the annealing simulations did not show any significant effect of initial orientation (up or down) for the *holo* form, there is a distinction for the *apo* form, where the **Down** orientation produced a greater number of adsorbed bases. Over the four runs, the *holo* form yielded a greater number of adsorbed bases compared with the *apo* form (29 vs 25 bases). However, the variance between individual runs was still too great to conclusively demonstrate that this result is statistically significant.

DOI: 10.1021/acssensors.7b00435
ACS Sens. 2017, 2, 1602−1611

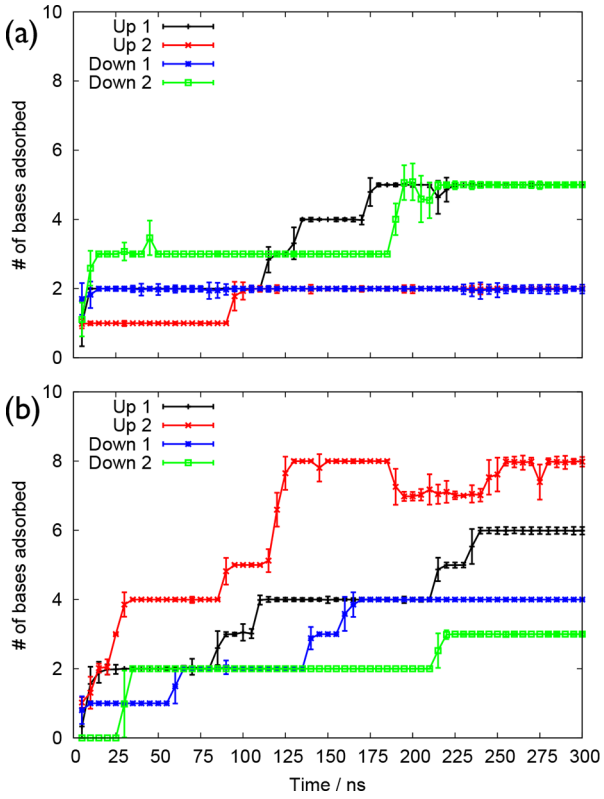

Figure 4. Number of nucleobases directly adsorbed to the graphene surface in the control simulations for (a) the *apo* and (b) the *holo* forms of the aptamer.

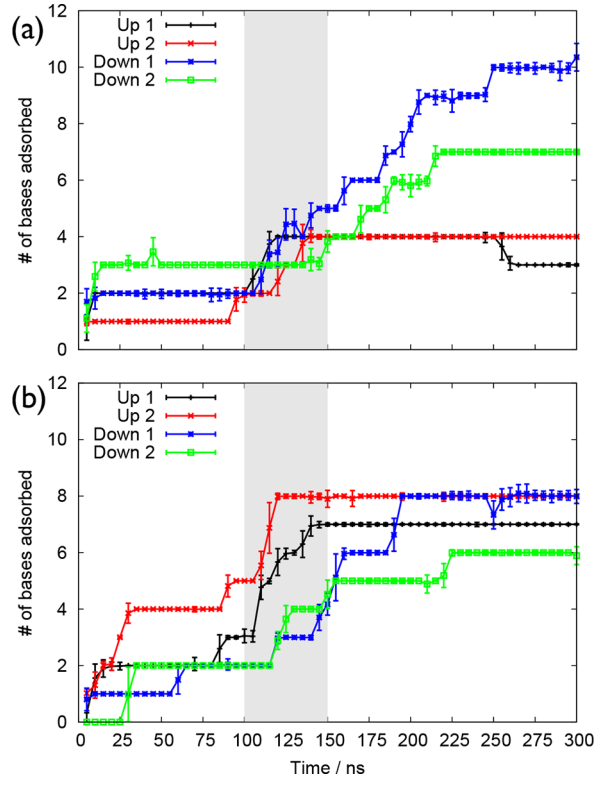

Figure 5. Number of nucleobases directly adsorbed to the graphene surface in the annealing simulations as a function of simulation time for (a) the *apo* and (b) the *holo* forms of the aptamer.

As mentioned earlier, previously reported simulations of DNA adsorbed at aqueous graphene interfaces have shown that ssDNA and dsDNA support different adsorption modes, with ssDNA typically featuring a large proportion of nucleobases directly adsorbed on the surface, while dsDNA is often reported as adsorbed to these substrates either indirectly, or directly only via the terminal bases. In general, an aptamer might be expected to support a mixture of both types of binding modality, because aptamers tend to feature regions of both ssDNA and duplex characteristics. To elaborate, while there are typically regions of strong intrabase interaction in a given aptamer, there may also be ssDNA-like regions, such as the analyte binding site, where surface adsorption may be likely.

In addition to the bases in the vicinity of the binding pocket, other regions in this aptamer may also be susceptible to adsorption at the graphite surface. These regions include the terminal pair of nucleobases at the open end of the stem (A1 and T27) and the bases in the small loop at the distal end of the aptamer (A13-T14-T15). In fact, nucleobases from all three of these locations within the aptamer adsorbed at the graphene interface, although each individual simulation may only support adsorption at one or two of these locations. Tables S2 and S3 in the Supporting Information summarize the location of nucleobases adsorbed resulting from each simulation. Figure 6 provides a selection of snapshots of the final configurations from different simulations, illustrating some of the variety of different binding modes that the aptamer supported when adsorbed at the aqueous graphene interface. Representative snapshots of the final configurations from all surface-adsorbed runs are provided in Figures S5−S8 of the Supporting Information. The selected snapshots shown in Figure 6 include conformations with only the terminal nucleobases (A1 and T27) bound to the surface (where the long axis of the aptamer is approximately perpendicular to the surface plane (Figure 6a), conformations where the aptamer is adsorbed in a parallel fashion (Figure 6b,d) and geometries where direct surface contact is primarily mediated via the bases in the binding pocket (Figure 6c).

The data summarized in Table S3, alongside Figure 5, offers a possible explanation for the differences observed between the **Up** and **Down** orientations of the *apo* form. For the simulations started in **Up** orientation, the adsorbed nucleobases were chiefly located in the head and tail regions of the aptamer. In contrast, for the simulations started in the **Down** orientation, a large proportion of the adsorbed bases were located in the central region of the aptamer corresponding with the position of the binding pockets. This is understandable because the simulations started in the **Down** orientation positioned the binding pocket directed toward the graphene surface, while in the **Up** orientation the center of the aptamer was instead exposed to the solution (see Figure 1). In the case of the *holo* form in the **Down** orientation, we propose that the presence of the adenosine molecules may hinder the adsorption of nucleobases in this location, even if in some instances the adenosine molecules escaped from the aptamer pocket (as described below).

For the control simulations started from the **Up** orientation, none of the four adenosine molecules (two per aptamer, over two simulations) became unbound. However, for the simulations started from the **Down** orientation, one adenosine molecule in one run became unbound and instead became bound to the graphene surface. For the annealing runs, both ligands were expelled from the binding pocket in all but one

DOI: 10.1021/acssensors.7b00435
ACS Sens. 2017, 2, 1602−1611

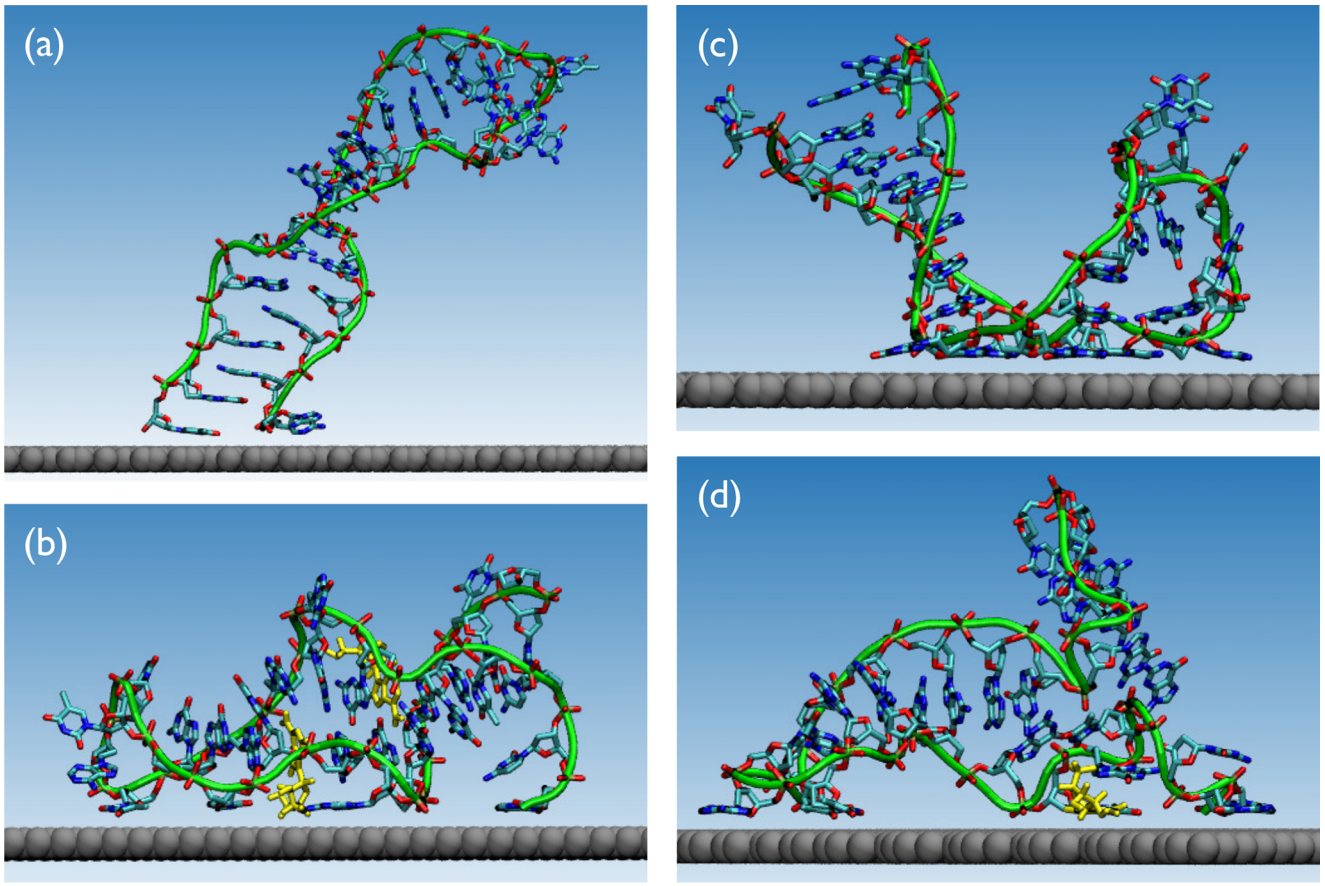

Figure 6. Snapshots of representative configurations of (a,c) the *apo* and (b,d) the *holo* forms from the control (a,b) and annealing (c,d) simulations. Snapshots were taken from simulations starting in the **Down** configuration. Water molecules and hydrogen atoms in the aptamer are not shown for clarity. Color code: graphene surface in gray, adenosine molecules in yellow, aptamer backbone in green, while the carbon, nitrogen, and oxygen atoms of the aptamer are colored cyan, blue, and red, respectively.

run (in the **Up** orientation). After detaching from the binding pocket, the adenosine molecules quickly (and on the time scales of the simulations irreversibly) adsorbed to the graphene surface, and typically interacted with adsorbed bases of the aptamer. In summary, these simulations suggest that the adsorption of the aptamer to the aqueous graphene interface might interfere with the binding of the analyte in the binding pocket, particularly if the molecule is adsorbed in a **Down** orientation. This suggests that modifications to this aptamer, namely, incorporation of an additional surface-binding sequence located away from the binding pockets, may encourage aptamer adsorption via regions distant from the adenosine binding sites.

The variation of the backbone RMSD, number of intrabase H-bonds, and base stacking number for all the simulation runs of the surface-adsorbed systems (averaged over all four runs for each system) are shown Figure 7, while the corresponding data for each individual run are shown in Figures S9–S12 of the Supporting Information. As already noted for the aptamer in bulk solution, the control simulations of the adsorbed aptamer showed only minor variation in these metrics over the 300 ns duration, with the *apo* showing a small but statistically significant increase in RMSD and decrease in the number of base–base hydrogen bonds. The SA procedure induced a similar disruption to the intramolecular structure of the aptamer, as also seen for the aptamer in bulk solution, captured by a decrease in the intrabase hydrogen bonding and base stacking number, along with an increase in the backbone RMSD. The large differences between runs have resulted in large calculated uncertainties, but on average the backbone RMSD was greater for the *apo* form than the *holo* form. By comparison of the results of the surface-adsorbed systems against the aptamer free in bulk solution, no statistically significant differences are observed, confirming that even in the adsorbed state substantial intramolecular interactions were present in this aptamer.

We remark here on two aspects of our simulations that merit further discussion. The first is the degree of conformational sampling, particularly for the surface-adsorbed aptamer. While our SA approach appeared to yield better performance compared with standard MD simulations in terms of exploring the configurations of the surface-bound aptamer, we also recognize that alternative approaches should be effective. To this end, we performed some preliminary investigations of DNA adsorbed at the aqueous graphene interface using Replica Exchange with Solute Tempering (REST)[63] MD simulations, based on our experience with this approach as applied to aqueous peptide–surface interfaces.[64] The outcomes from our preliminary simulations, detailed in the Supporting Information section Comparison of Simulated Annealing and REST Approaches, do not suggest that REST-MD simulations are more effective than SA in this instance, especially given the greater computational expense compared with the SA approach. Nonetheless, we emphasize the preliminary character of these

DOI: 10.1021/acssensors.7b00435
ACS Sens. 2017, 2, 1602–1611

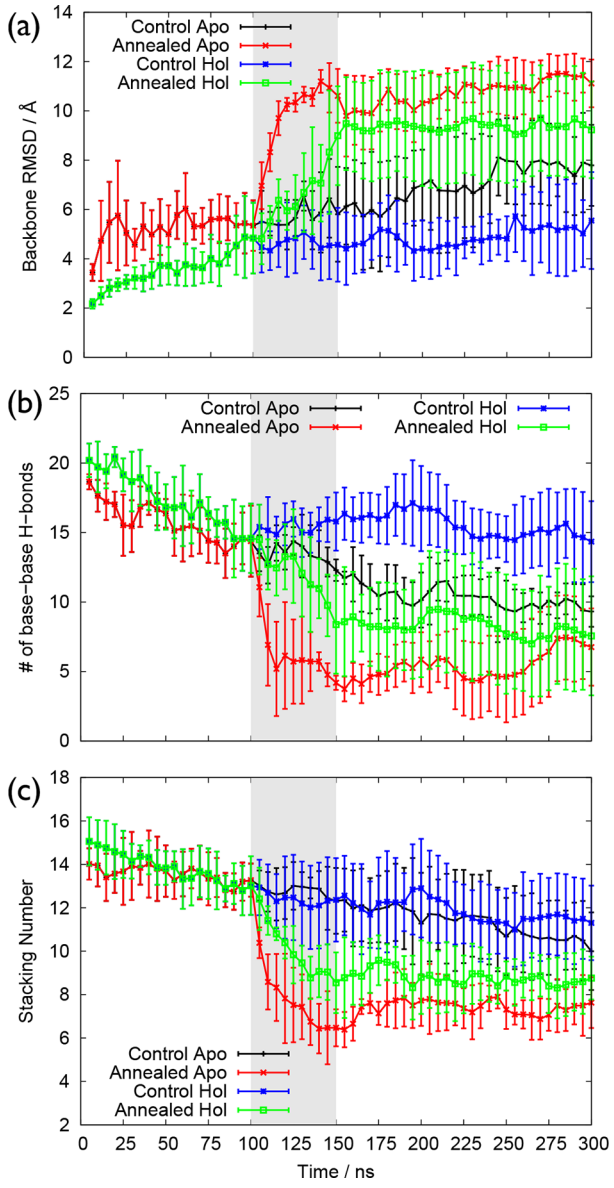

Figure 7. Results of simulations of the DNA aptamer adsorbed at the aqueous graphene interface, averaged over four runs for each system: (a) the RMSD of the backbone atoms of the aptamer, (b) the number of DNA nucleobase−nucleobase hydrogen bonds, and (c) the base stacking number as a function of simulation time. The shaded area shows the period where the simulated annealing protocol was applied to the annealed runs.

findings, and suggest that future efforts could be profitably directed into optimizing and refining the parameters and implementation of the REST-MD simulation approach as applied to surface-adsorbed aptamers.

The second aspect of our simulations that warrants further discussion is the influence of salt concentration. We reiterate here that we deliberately chose to model our DNA/graphene interfaces in a NaCl solution with a concentration of 0.05 mol kg^{-1} so as to align with previously reported SMFS experimental conditions.[21] However, we recognize that salt effects are of general interest for aptasensor design. In light of this, we conducted a preliminary investigation of the conformation of the aptamer at a higher salt solution concentration. The outcomes from this preliminary work (summarized in the Supporting Information section Effect of Salt Concentration) indicate that our analysis metrics (such as the number of intrabase hydrogen bonds and the stacking number) were not dramatically affected at the higher salt concentration. However, we again emphasize the preliminary nature of these results and suggest that a more in-depth investigation of the influence of salt concentration would be valuable.

The previously published SMFS experiments of this aptamer adsorbed at aqueous graphite provide the most relevant basis for comparison with our simulation results. These previous SMFS experiments reported that a greater force was required to detach the aptamer from the aqueous graphene interface after the addition of adenosine, compared with the peeling force of the surface-adsorbed aptamer in the absence of adenosine.[21] Moreover, this effect was only observed for adenosine, i.e., the addition of other nucleosides did not lead to any increase in the peeling force. Li et al. explained this by proposing that the *apo* form would follow a ssDNA-like adsorption mode, with most of the base in direct contact with the graphene substrate, such that the bases would successively desorb (one by one) when subjected to the peeling force. Furthermore, these authors also hypothesized that, in the *holo* form (in the presence of adenosine), the presence of the adenosines in the binding pockets may hinder this successive, base-by-base detachment process, and therefore would require a greater force to desorb the aptamer from the surface.

In contrast with this hypothesis from Li et al.,[21] the results of our simulations suggest that even the *apo* form retained a substantial amount of secondary structure when adsorbed at the aqueous graphene interface. In this case, more than half of the bases were not directly bound to the surface. However, one complication in comparing our simulations with the current experimental data is the role of adenosine (or the other nucleosides that were added in the control experiments). To elaborate, in the SMFS experiments the sample cell was first filled with the analyte solution, and following this the aptamer-functionalized AFM probe was submerged in this solution for 1 h, prior to being lowered into contact with the graphite (HOPG) substrate. Our simulation results suggest that the graphite substrate could compete with the aptamer for the binding of the adenosine molecules present in the solution.

Both simulation and experiment suggest that adenosine binds strongly at the aqueous graphene interface.[16,19,22,55] This binding strength, ranging from −41 to −24 kJ mol^{-1}, is competitive with (or exceeds) the experimentally determined adenosine-aptamer binding strength of −27 kJ mol^{-1}.[37] However, aptamers that target analytes other an adenosine may quite likely face less competition from the graphene substrate. Therefore, is possible in these experiments that the nucleosides in the solution adsorbed to the HOPG substrate prior to the aptamer binding event, and these preadsorbed nucleosides might have interacted with the nucleobases in the aptamer. In fact, previous simulations have shown that nucleobase dimers adsorbed at aqueous graphene interfaces can be stabilized via hydrogen bonding (both WC and non-WC).[15,17] Therefore, the force required to desorb the aptamer in the presence of adenosine may be due to the presence of substrate-bound adenosine molecules, which could conceivably strengthen the interaction of aptamer with the substrate. However, how and why such an effect is not observed in the presence of other nucleosides in solution is a question that requires further investigation, both experimental and modeling, to address.

DOI: 10.1021/acssensors.7b00435
ACS Sens. 2017, 2, 1602−1611

In closing, our simulation data indicate that considerable complexity is inherent to the aqueous aptamer−surface interface. Definitive resolution, in terms of the conformational ensemble of these surface-adsorbed aptamers, and the possible influence of this ensemble on the sensing traits of these interfaces, can only be achieved via a partnership of simulation and experimental approaches. MD simulation data such as those detailed in this work may in turn prompt advances in the experimental characterization of these challenging interfaces, to enable rational knowledge-based strategies for optimizing aptasensor design.

CONCLUSIONS

We used molecular dynamics simulations to predict the structure and properties of the adenosine-binding DNA aptamer in the presence and absence of the target analyte, both when free in bulk solution and when adsorbed at the aqueous graphene interface. Our simulation results indicate that graphene adsorption can support a variety of different binding modes, with both terminal bases, the loop, and binding pockets susceptible to surface adsorption. However, the maximum number of adsorbed nucelobases did not exceed ten (37%), which is a smaller proportion of adsorbed bases than has been typically reported in simulations of unstructured ssDNA adsorbed at graphene interfaces. In addition, the strong intramolecular interactions present in the aptamer competed with the graphene−aptamer interactions, as has been previously reported for simulations of duplex DNA adsorption. Therefore, this aptamer exhibited a mixture of ssDNA-like and dsDNA-like adsorption modes, with substantial retention of intramolecular interactions. However, our simulations suggest that the binding affinity and selectivity of adenosine in some instances may be affected by the presence of the aqueous graphene interface. For some of the favorable adsorbed configurations predicted by our simulations, detachment of the adenosine analytes may have been facilitated by competition between adenosine−pocket and adenosine−graphene interactions. However, adenosine is thought to bind strongly at aqueous graphitic substrates, and therefore aptamers that target analytes other an adenosine may quite likely face less competition from the graphene substrate. Overall, our simulations indicate that while DNA aptamer-based devices have considerable potential, the balance of competitive interactions among the aptamer, the target analyte, and the substrate must be considered. Molecular dynamics simulations can provide valuable insights into this balance and therefore the choice and suitability of a device substrate with a given aptamer.

ASSOCIATED CONTENT

Supporting Information

The Supporting Information is available free of charge on the ACS Publications website at DOI: 10.1021/acssensors.7b00435.

Summary of simulations performed; analysis of structural parameters of aptamer in each individual simulation; summary of the number and location (base number) of graphene-adsorbed nucleobases (PDF)

AUTHOR INFORMATION

Corresponding Author

*E-mail: tiffany.walsh@deakin.edu.au.

ORCID

Zak E. Hughes: 0000-0003-2166-9822
Tiffany R. Walsh: 0000-0002-0233-9484

Notes

The authors declare no competing financial interest.

ACKNOWLEDGMENTS

This research was supported in part by the Asian Office of Aerospace Research and Development (AOARD), grant number FA2386-16-1-4053. We are grateful for computational resources provided by the Victorian Life Sciences Computation Initiative (VLSCI) and the Pawsey Supercomputing Centre, with funding from the Australian Government and the Government of Western Australia.

REFERENCES

(1) Ellington, A. D.; Szostak, J. W. In vitro selection of RNA molecules that bind specific ligands. *Nature* **1990**, *346*, 818−822.
(2) Breaker, R. R. DNA aptamers and DNA enzymes. *Curr. Opin. Chem. Biol.* **1997**, *1*, 26−31.
(3) Hermann, T.; Patel, D. J. Adaptive recognition by nucleic acid aptamers. *Science* **2000**, *287*, 820−825.
(4) Tan, W.; Donovan, M. J.; Jiang, J. Aptamers from Cell-Based Selection for Bioanalytical Applications. *Chem. Rev.* **2013**, *113*, 2842−2862.
(5) Sun, H.; Zhu, X.; Lu, P. Y.; Rosato, R. R.; Tan, W.; Zu, Y. Oligonucleotide Aptamers: New Tools for Targeted Cancer Therapy. *Mol. Ther.–Nucleic Acids* **2014**, *3*, e182.
(6) Meng, H.-M.; Liu, H.; Kuai, H.; Peng, R.; Mo, L.; Zhang, X.-B. Aptamer-integrated DNA nanostructures for biosensing, bioimaging and cancer therapy. *Chem. Soc. Rev.* **2016**, *45*, 2583−2602.
(7) Li, H.; Rothberg, L. *Proc. Natl. Acad. Sci. U. S. A.* **2004**, *101*, 14036−14039.
(8) Chang, H.; Tang, L.; Wang, Y.; Jiang, J.; Li, J. Graphene Fluorescence Resonance Energy Transfer Aptasensor for the Thrombin Detection. *Anal. Chem.* **2010**, *82*, 2341−2346.
(9) Serrano-Santos, M. B.; Llobet, E.; Özalp, V. C.; Schäfer, T. Characterization of structural changes in aptamer films for controlled release nanodevices. *Chem. Commun.* **2012**, *48*, 10087−10089.
(10) Liu, Z.; Chen, S.; Liu, B.; Wu, J.; Zhou, Y.; He, L.; Ding, J.; Liu, J. Intracellular Detection of ATP Using an Aptamer Beacon Covalently Linked to Graphene Oxide Resisting Nonspecific Probe Displacement. *Anal. Chem.* **2014**, *86*, 12229−12235.
(11) Tang, L.; Wang, Y.; Li, J. The graphene/nucleic acid nanobiointerface. *Chem. Soc. Rev.* **2015**, *44*, 6954−6980.
(12) Manohar, S.; Mantz, A. R.; Bancroft, K. E.; Hui, C.-Y.; Jagota, A.; Vezenov, D. V. Peeling Single-Stranded DNA from Graphite Surface to Determine Oligonucleotide Binding Energy by Force Spectroscopy. *Nano Lett.* **2008**, *8*, 4365−4372.
(13) Johnson, R. R.; Johnson, A. T. C.; Klein, M. L. The nature of DNA-base-carbon-nanotube interactions. *Small* **2010**, *6*, 31−34.
(14) Lulevich, V.; Kim, S.; Grigoropoulos, C. P.; Noy, A. Frictionless Sliding of Single-Stranded DNA in a Carbon Nanotube Pore Observed by Single Molecule Force Spectroscopy. *Nano Lett.* **2011**, *11*, 1171−1176.
(15) Spiwok, V.; Hobza, P.; Řezáč, J. Free-Energy Simulations of Hydrogen Bonding versus Stacking of Nucleobases on a Graphene Surface. *J. Phys. Chem. C* **2011**, *115*, 19455−19462.
(16) Iliafar, S.; Wagner, K.; Manohar, S.; Jagota, A.; Vezenov, D. Quantifying Interactions between DNA Oligomers and Graphite Surface Using Single Molecule Force Spectroscopy. *J. Phys. Chem. C* **2012**, *116*, 13896−13903.
(17) Shankar, A.; Jagota, A.; Mittal, J. DNA Base Dimers Are Stabilized by Hydrogen-Bonding Interactions Including Non-Watson-Crick Pairing Near Graphite Surfaces. *J. Phys. Chem. B* **2012**, *116*, 12088−12094.

DOI: 10.1021/acssensors.7b00435
ACS Sens. 2017, 2, 1602−1611

(18) Wei, G.; Steckbeck, S.; Köppen, S.; Colombi Ciacchi, L. Label-free biosensing with single-molecule force spectroscopy. *Chem. Commun.* **2013**, *49*, 3239−3241.
(19) Iliafar, S.; Mittal, J.; Vezenov, D.; Jagota, A. Interaction of Single-Stranded DNA with Curved Carbon Nanotube is Much Stronger than with Flat Graphite. *J. Am. Chem. Soc.* **2014**, *136*, 12947−12957.
(20) Wei, G.; Li, Q.; Steckbeck, S.; Colombi Ciacchi, L. Direct force measurements on peeling heteropolymer ssDNA from a graphite surface using single-molecule force spectroscopy. *Phys. Chem. Chem. Phys.* **2014**, *16*, 3995−4001.
(21) Li, J.; Li, Q.; Colombi Ciacchi, L.; Wei, G. Label-Free Sensing of Adenosine Based on Force Variations Induced by Molecular Recognition. *Biosensors* **2015**, *5*, 85−97.
(22) Ranganathan, S. V.; Halvorsen, K.; Myers, C. A.; Robertson, N. M.; Yigit, M. V.; Chen, A. A. Complex Thermodynamic Behavior of Single-Stranded Nucleic Acid Adsorption to Graphene Surfaces. *Langmuir* **2016**, *32*, 6028−6034.
(23) Roxbury, D.; Jagota, A.; Mittal, J. Sequence-Specific Self-Stitching Motif of Short Single-Stranded DNA on a Single-Walled Carbon Nanotube. *J. Am. Chem. Soc.* **2011**, *133*, 13545−13550.
(24) Roxbury, D.; Mittal, J.; Jagota, A. Molecular-Basis of Single-Walled Carbon Nanotube Recognition by Single-Stranded DNA. *Nano Lett.* **2012**, *12*, 1464−1469.
(25) Martin, W.; Zhu, W.; Krilov, G. Simulation Study of Noncovalent Hybridization of Carbon Nanotubes by Single-Stranded DNA in Water. *J. Phys. Chem. B* **2008**, *112*, 16076−16089.
(26) Manna, A. K.; Pati, S. K. Theoretical understanding of single-stranded DNA assisted dispersion of graphene. *J. Mater. Chem. B* **2013**, *1*, 91−100.
(27) Kabeláč, M.; Kroutil, O.; Předota, M.; Lankaš, F.; Šíp, M. Influence of a charged graphene surface on the orientation and conformation of covalently attached oligonucleotides: a molecular dynamics study. *Phys. Chem. Chem. Phys.* **2012**, *14*, 4217−4229.
(28) Ghosh, S.; Patel, N.; Chakrabarti, R. Probing the Salt Concentration Dependent Nucleobase Distribution in a Single-Stranded DNA-Single-Walled Carbon Nanotube Hybrid with Molecular Dynamics. *J. Phys. Chem. B* **2016**, *120*, 455−466.
(29) Zeng, S.; Chen, L.; Wang, Y.; Chen, J. Exploration on the mechanism of DNA adsorption on graphene and graphene oxide via molecular simulations. *J. Phys. D: Appl. Phys.* **2015**, *48*, 275402.
(30) Zhao, X.; Johnson, J. K. Simulation of adsorption of DNA on carbon nanotubes. *J. Am. Chem. Soc.* **2007**, *129*, 10438−10445.
(31) Wu, M.; Kempaiah, R.; Huang, P.-J. J.; Maheshwari, V.; Liu, J. Adsorption and Desorption of DNA on Graphene Oxide Studied by Fluorescently Labeled Oligonucleotides. *Langmuir* **2011**, *27*, 2731−2738.
(32) Zhao, X. Self-Assembly of DNA Segments on Graphene and Carbon Nanotube Arrays in Aqueous Solution: A Molecular Simulation Study. *J. Phys. Chem. C* **2011**, *115*, 6181−6189.
(33) Botti, S.; Rufoloni, A.; Laurenzi, S.; Gay, S.; Rindzevicius, T.; Schmidt, M. S.; Santonicola, M. G. DNA self-assembly on graphene surface studied by SERS mapping. *Carbon* **2016**, *109*, 363−372.
(34) Huizenga, D. E.; Szostak, J. W. A DNA aptamer that binds adenosine and ATP. *Biochemistry* **1995**, *34*, 656−665.
(35) Lin, C. H.; Patei, D. J. Structural basis of DNA folding and recognition in an AMP-DNA aptamer complex: distinct architectures but common recognition motifs for DNA and RNA aptamers complexed to AMP. *Chem. Biol.* **1997**, *4*, 817−832.
(36) Xia, T.; Yuan, J.; Fang, X. Conformational dynamics of an ATP-binding DNA aptamer: a single-molecule study. *J. Phys. Chem. B* **2013**, *117*, 14994−15003.
(37) Zhang, Z. J.; Oni, O.; Liu, J. W. New insights into a classic aptamer: binding sites, cooperativity and more sensitive adenosine detection. *Nucleic Acids Res.* **2017**, *45*, 7593−7601.
(38) Datta, D.; Meshik, X.; Mukherjee, S.; Sarkar, K.; Choi, M. S.; Mazouchi, M.; Farid, S.; Wang, Y. Y.; Burke, P. J.; Dutta, M.; Stroscio, M. A. Submillimolar Detection of Adenosine Monophosphate Using Graphene-Based Electrochemical Aptasensor. *IEEE Trans. Nanotechnol.* **2017**, *16*, 196−202.
(39) Lee, O.-S.; Schatz, G. C. Interaction between DNAs on a Gold Surface. *J. Phys. Chem. C* **2009**, *113*, 15941−15947.
(40) Lee, O.-S.; Schatz, G. C. Molecular Dynamics Simulation of DNA-Functionalized Gold Nanoparticles. *J. Phys. Chem. C* **2009**, *113*, 2316−2321.
(41) Wang, G. M.; Sandberg, W. C. Complete all-atom hydrodynamics of protein unfolding in uniform flow. *Nanotechnology* **2010**, *21*, 235101.
(42) Rosa, M.; Corni, S.; Di Felice, R. Enthalpy-Entropy Tuning in the Adsorption of Nucleobases at the Au(111) Surface. *J. Chem. Theory Comput.* **2014**, *10*, 1707−1716.
(43) Roxbury, D.; Manohar, S.; Jagota, A. Molecular Simulation of DNA β-Sheet and β-Barrel Structures on Graphite and Carbon Nanotubes. *J. Phys. Chem. C* **2010**, *114*, 13267−13276.
(44) Li, N. K.; Kim, H. S.; Nash, J. A.; Lim, M.; Yingling, Y. G. Progress in molecular modelling of DNA materials. *Mol. Simul.* **2014**, *40*, 777.
(45) Kong, Z.; Zheng, W.; Wang, Q.; Wang, H.; Xi, F. Charge-tunable absorption behavior of DNA on graphene. *J. Mater. Chem. B* **2015**, *3*, 4814−4820.
(46) Landry, M. P.; Vuković, L.; Kruss, S.; Bisker, G.; Landry, A. M.; Islam, S.; Jain, R.; Schulten, K.; Strano, M. S. Comparative Dynamics and Sequence Dependence of DNA and RNA Binding to Single Walled Carbon Nanotubes. *J. Phys. Chem. C* **2015**, *119*, 10048−10058.
(47) Qamhieh, K.; Wong, K. Y.; Lynch, G. C.; Pettitt, B. M. The melting mechanism of DNA tethered to a surface. *Int. J. Num. Anal. Modeling* **2009**, *6*, 474−488.
(48) Swadling, J. B.; Coveney, P. V.; Greenwell, H. C. Clay Minerals Mediate Folding and Regioselective Interactions of RNA: A Large-Scale Atomistic Simulation Study. *J. Am. Chem. Soc.* **2010**, *132*, 13750−13764.
(49) Elder, R. M.; Pfaendtner, J.; Jayaraman, A. Effect of Hydrophobic and Hydrophilic Surfaces on the Stability of Double-Stranded DNA. *Biomacromolecules* **2015**, *16*, 1862−1869.
(50) Foloppe, N.; MacKerell, A. D., Jr All-atom empirical force field for nucleic acids: I. Parameter optimization based on small molecule and condensed phase macromolecular target data. *J. Comput. Chem.* **2000**, *21*, 86−104.
(51) MacKerell, A. D.; Banavali, N. K. All-atom empirical force field for nucleic acids: II. Application to molecular dynamics simulations of DNA and RNA in solution. *J. Comput. Chem.* **2000**, *21*, 105−120.
(52) Jorgensen, W. L.; Chandrasekhar, J.; Madura, J. D.; Impey, R. W.; Klein, M. L. Comparison of simple potential functions for simulating liquid water. *J. Chem. Phys.* **1983**, *79*, 926.
(53) Neria, E.; Fischer, S.; Karplus, M. Simulation of activation free energies in molecular systems. *J. Chem. Phys.* **1996**, *105*, 1902−1921.
(54) Hughes, Z. E.; Tomásio, S. M.; Walsh, T. R. Efficient simulations of the aqueous bio-interface of graphitic nanostructures with a polarisable model. *Nanoscale* **2014**, *6*, 5438−5448.
(55) Hughes, Z. E.; Wei, G.; Drew, K. L. M.; Colombi Ciacchi, L.; Walsh, T. R. Adsorption of DNA Fragments at Aqueous Graphite and Au(111) via Integration of Experiment and Simulation. *Langmuir* **2017**, *33*, 10193−10204.
(56) Abraham, M. J.; Murtola, T.; Schulz, R.; Páll, S.; Smith, J. C.; Hess, B.; Lindahl, E. GROMACS: High performance molecular simulations through multi-level parallelism from laptops to supercomputers. *SoftwareX* **2015**, *1−2*, 19−25.
(57) Darden, T.; York, D.; Pedersen, L. Particle Mesh Ewald - an N.Log(N) Method for Ewald Sums in Large Systems. *J. Chem. Phys.* **1993**, *98*, 10089−10092.
(58) Nosé, S. A unified formulation of the constant temperature molecular dynamics methods. *J. Chem. Phys.* **1984**, *81*, 511−519.
(59) Hoover, W. Canonical dynamics: Equilibrium phase-space distributions. *Phys. Rev. A: At., Mol., Opt. Phys.* **1985**, *31*, 1695−1697.
(60) Parrinello, M.; Rahman, A. Polymorphic transitions in single crystals: A new molecular dynamics method. *J. Appl. Phys.* **1981**, *52*, 7182−7190.

DOI: 10.1021/acssensors.7b00435
ACS Sens. 2017, 2, 1602−1611

(61) Portella, G.; Orozco, M. Multiple Routes to Characterize the Folding of a Small DNA Hairpin. *Angew. Chem., Int. Ed.* **2010**, *49*, 7673−7676.
(62) Hughes, Z. E.; Walsh, T. R. What makes a good graphene-binding peptide? Adsorption of amino acids and peptides at aqueous graphene interfaces. *J. Mater. Chem. B* **2015**, *3*, 3211−3221.
(63) Terakawa, T.; Kameda, T.; Takada, S. On easy implementation of a variant of the replica exchange with solute tempering in GROMACS. *J. Comput. Chem.* **2011**, *32*, 1228−1234.
(64) Wright, L. B.; Walsh, T. R. Efficient conformational sampling of peptides adsorbed onto inorganic surfaces: insights from a quartz binding peptide. *Phys. Chem. Chem. Phys.* **2013**, *15*, 4715−4726.

DOI: 10.1021/acssensors.7b00435
ACS Sens. 2017, 2, 1602−1611